

# Realization of efficient electroabsorption using intersubband transitions in step quantum wells

P. Holmström,<sup>1\*</sup> P. Jänes,<sup>1,2</sup> U. Ekenberg<sup>1</sup> and L. Thylén<sup>1</sup>

<sup>1</sup>Laboratory of Photonics and Microwave Engineering,  
Department of Microelectronics and Applied Physics,

Royal Institute of Technology (KTH), SE-164 40 Kista, Sweden.

<sup>2</sup>Present address: Proximion Fiber Systems AB, SE-16440 Kista, Sweden.

(Dated: February 2, 2008)

We have demonstrated efficient intersubband electroabsorption in InGaAs/InAlGaAs/InAlAs step quantum wells grown by metal-organic vapor phase epitaxy (MOVPE). An absorption modulation of 6 dB at  $\lambda = 6.0 \mu\text{m}$  due to Stark shift of the IS absorption was achieved at a low voltage swing of  $\pm 0.5 \text{ V}$  in a multipass waveguide structure. Based on the experimental results it is estimated that an electroabsorption modulator with a low peak-to-peak voltage of  $V_{\text{pp}} = 0.9 \text{ V}$  can yield a modulation speed of  $f_{3\text{dB}} \approx 120 \text{ GHz}$  with the present material by using a strongly confining surface plasmon waveguide of  $30 \mu\text{m}$  length.

Intersubband (IS) transitions have primarily been applied to quantum-well infrared photodetectors (QWIPs)<sup>1</sup> and quantum cascade lasers (QCLs).<sup>2</sup> However, the properties of IS transitions are also attractive for application to electroabsorption (EA) modulators. A fundamental advantage of intersubband transitions is that the electron subbands are essentially parallel to each other. The weak dependence on the in-plane wave vector results in sharply peaked IS resonances and a potential for strong absorption implying compact modulators. The broadening of the peaks due to subband nonparabolicity has been shown to be effectively cancelled by collective phenomena.<sup>3</sup> A small IS absorption linewidth  $\Gamma$  is imperative for a high RC-limited speed in IS-based EA-modulators, as generally the modulator capacitance  $C \sim \Gamma^3$ .<sup>[4]</sup> Other advantages are the rapid IS relaxation time of only  $\sim 1 \text{ ps}$  which enables saturation resistant modulators, and the possibility to achieve a negative chirp parameter.

IS based modulation has previously been demonstrated at mid-IR wavelengths,<sup>5,6</sup> however using rather large voltages. In this letter we show experimentally that an absorption modulation of 6 dB at  $\lambda = 6.0 \mu\text{m}$  due to Stark shift of the IS absorption can be achieved with a voltage swing as low as  $\pm 0.5 \text{ V}$ . Based on these results we estimate that an electroabsorption modulator with a low peak-to-peak voltage of  $V_{\text{pp}} = 0.9 \text{ V}$  can yield a modulation speed of  $f_{3\text{dB}} \approx 120 \text{ GHz}$  with the present material by using a strongly confining surface plasmon waveguide of  $30 \mu\text{m}$  length.

The samples were grown in an Aixtron AIX-200 MOVPE system on semi-insulating InP:Fe substrates. First a 500 nm n-InP ( $5 \times 10^{17} \text{ cm}^{-3}$ ) buffer layer was grown. It was followed by a 60 nm lattice-matched n-AlGaInAs ( $x_{\text{Al}}=0.37$ ,  $5 \times 10^{17} \text{ cm}^{-3}$ ) layer, which was grown immediately before the MQW layer, with a similar one just after the MQW. The purpose of these two

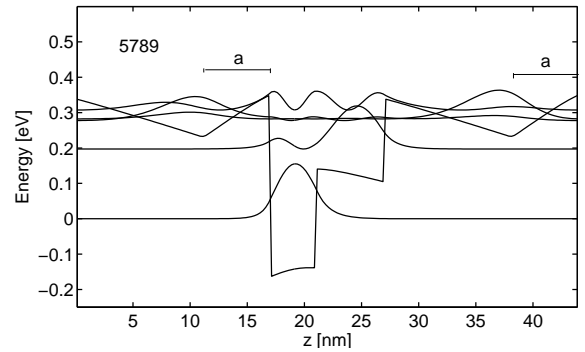


FIG. 1: Potential profile of the step QW in the sample 5789 with no applied bias voltage. Also shown are the moduli squared of the bound states in the step QW as well as two mostly barrier confined states. The samples differ by the thickness  $a$  of the spacer layer between the  $\delta$ -doping layer and the InGaAs QW layer.  $a = 5.6 \text{ nm}$  and  $8.3 \text{ nm}$  in the samples 5789 and 5791, respectively.

n-AlGaInAs layers is to line up the Fermi energies inside and outside the MQW without bend bending,<sup>4</sup> in order to obtain the same IS transition energies in all step QWs. On top of the upper 60 nm n-AlGaInAs layer a 550 nm n-InP ( $5 \times 10^{17} \text{ cm}^{-3}$ ) cap layer was grown. Each step QW consists of a 4.0 nm InGaAs well layer, a 6.0 nm AlGaInAs step layer, separated by 16.7 nm InAlAs barrier layers. The barriers were Si  $\delta$ -doped at  $n_{\text{D}} = 2.2 \times 10^{12} \text{ cm}^{-2}$  to supply electrons in the step QWs. The  $\delta$ -dopings were performed by halting the growth while supplying  $\text{SiH}_4$ , whereafter the growth proceeded without further delay. Each sample had an MQW comprising 10 step QWs. Two samples 5789 and 5791 were grown which differed by the position of the  $\delta$ -doping layer. The potential profile of one step QW in 5789 without any applied bias voltage is shown in Fig. 1.

Structural characterization of the grown samples was performed by a combination of high-resolution X-ray diffraction (XRD) measurements and simulation of the two observed IS resonance peak energies  $\tilde{E}_{12}$  and  $\tilde{E}_{13}$ .

\*Electronic mail: petterh@kth.se

By XRD  $2\theta - \omega$  scans the MQW period  $L_p = 26.7 \pm 0.2$  nm in the samples could be reliably obtained. But since the MQW comprises a repetition of three different and nearly lattice-matched layers, viz. the InGaAs well layer, the InAlGaAs step layer and the InAlAs barrier, the individual thicknesses and compositions of these were not available from XRD results alone. However the IS peak energies  $\bar{E}_{12}$  and  $\bar{E}_{13}$  as well as the ratio between the two oscillator strengths  $f_{13}/f_{12}$  adds enough information to determine the thickness of the well and step layers as well as the conduction band edge of the step layer corresponding to a composition of  $\text{Al}_{0.30}\text{Ga}_{0.18}\text{In}_{0.52}\text{As}$ .

The IS transition energies were modeled in the envelope function approximation. The structures examined here in many respects coincide with the one we previously evaluated in a modulator simulation.<sup>4</sup> We have considered the nonparabolicity of the conduction band.<sup>7</sup> We solved for the step QW potential self-consistently including the Hartree space-charge potential and an exchange-correlation potential.<sup>8,9</sup> The exchange-correlation effects were thus included as a one-particle exchange-correlation potential. Further we also considered the collective shift of the IS resonance peak due to the depolarization and exciton effects.<sup>10</sup> Material parameters were obtained from the review paper by Vurgaftman *et al.*<sup>11</sup>

The IS absorption was characterized in a multi-pass geometry in the usual fashion where two bevelled edges and the back side of a  $5 \times 7$  mm piece were polished to allow multiple internal reflections. The spectra were measured using Fourier-transform infrared (FTIR) spectroscopy, and isolation of the IS absorbance was achieved by taking the ratio of the transmittance spectra of TM and TE-polarized light,  $A = -\log_{10}(T_{\text{TM}}/T_{\text{TE}})$ . In addition, a smooth background offset due to the polarization dependence in the FTIR spectrometer was subtracted. Due to polarization selection rules IS transitions almost exclusively couple to TM-polarized light. No significant absorption was observed for TE-polarized light.

To enable voltage to be applied over the MQWs Ti/Pt/Au contacts were deposited on the n-InP cap layer and on the buffer n-InP layer below the MQW stack. The bottom contact was deposited after lithography and dry-etching down to the bottom contact layer. The contacts were performed as stripes  $5 \times 0.2$  mm<sup>2</sup> with a distance of 4 mm between them. At zero bias the peak widths did not differ much between 77 K and room temperature. Clear Stark shifts of the  $1 \rightarrow 2$  and  $1 \rightarrow 3$  IS resonances were observed at low applied voltages, Fig. 2. The EA was characterized while keeping the samples in a liquid nitrogen cryostat at  $T=77$  K. Although the envisaged  $\mu\text{m}$ -scale ridge waveguide device should be operated at room-temperature, EA characterization at low temperature is necessary due to the large area of the multipass device. IV-characterization still revealed a significant leakage current. To obtain the part of the applied bias voltage  $V_b$  that was applied over the MQW it is thus necessary to account for the voltage drop in the contact layers. We model this by considering that

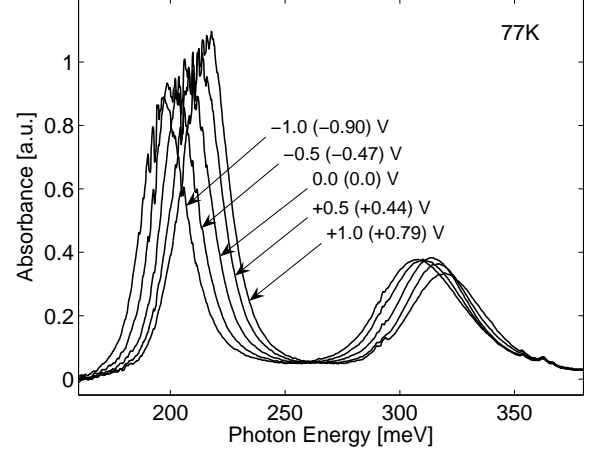


FIG. 2: Intersubband absorption spectra measured in sample 5789 for different applied voltages at  $T=77$  K. Clear Stark shifts of the  $1 \rightarrow 2$  and  $1 \rightarrow 3$  IS resonances are observed. Indicated for each spectrum is the applied voltage  $V_b$  and within parentheses the voltage over the MQW  $V_{b,\text{MQW}}$ .

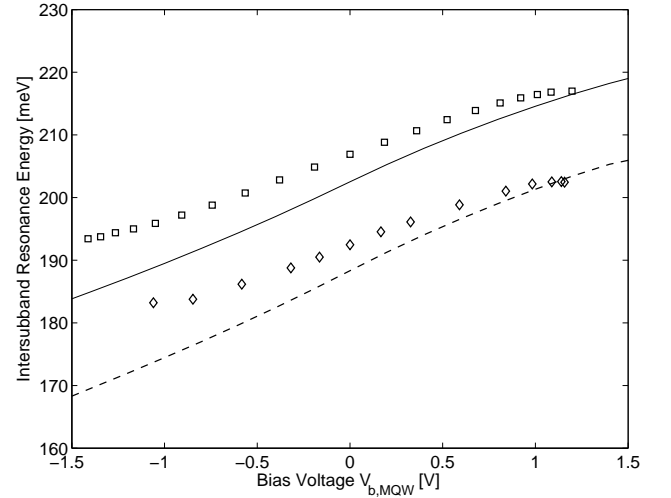


FIG. 3: Stark shift of the  $1 \rightarrow 2$  intersubband absorption peak position vs. the voltage  $V_{b,\text{MQW}}$  applied over the MQW. The symbols indicate experimental IS peak positions in the samples 5789 (squares) and 5791 (diamonds). The solid and dashed lines are the calculated Stark shift in the samples 5789 and 5791, respectively.

the device resistance  $R$  is composed of two parts in series  $R = R_{\text{lat}} + R_{\text{MQW}}$ . The resistance  $R_{\text{lat}}$  is associated with the lateral conduction in the n-InP contact layers and laterally in the MQW. We assume that  $R_{\text{lat}}$  is independent of the applied bias. The voltage that is applied over the MQW is then obtained by voltage division, i.e.  $V_{b,\text{MQW}} = V_b(R - R_{\text{lat}})/R$ . The bias dependent multi-pass device resistance  $R = V_b/I$ , where  $I$  is the current through the device.

The shift of the  $1 \rightarrow 2$  IS resonance due to the Stark effect in both the samples is shown in Fig. 3. The voltage

drop that occurred in the contact layers was compensated for by plotting the IS absorption peak positions vs. the voltage over the MQW,  $V_{b, \text{MQW}}$ . The experimental Stark shifts were still about 20% smaller than the calculated ones for sharp interfaces. Possible causes of the difference between the experimental and calculated Stark shifts are the uncertainty about the voltage drop outside the quantum well and intermixing of the QW interfaces. IS based structures have generally been grown by molecular-beam epitaxy (MBE) owing to its better control of small layer thicknesses and lower growth temperatures which should reduce interface intermixing. The present structures were, however, grown by metal-organic vapor-phase epitaxy (MOVPE) which is considered more suitable for commercial production.

Following ref.[4] we can predict the performance of high-speed modulators. Instead of a multi-pass geometry we then consider a surface plasmon waveguide. By having a heavily doped semiconductor layer below the MQW structure and Au above it we predicted that a modulator can be made as short as 30  $\mu\text{m}$ . In simulations for sharp interfaces we have predicted very high RC-limited room-temperature modulation speeds  $f_{3\text{dB}}$  at low voltages,<sup>4,12</sup> e.g.  $f_{3\text{dB}} \sim 190$  GHz at a driving voltage of only  $V_{\text{pp}} = 0.9$  V. Based on the experimental results in this paper it should still be possible to reach  $f_{3\text{dB}} \sim 120$  GHz.

High-speed IS modulators operating at  $\lambda = 6.0$   $\mu\text{m}$  can be useful for interconnects with Si waveguides. Si has a transmission window from 1.2 to 6.5  $\mu\text{m}$ .<sup>[13]</sup> The atmospheric absorption at the present wavelength is rather large. But with a slightly different design it should be

no problem to reach the windows at  $\lambda = 3 - 5$   $\mu\text{m}$  and  $\lambda = 8 - 12$   $\mu\text{m}$ . Such modulators would be very valuable for free-space communication.<sup>14</sup> This is an area of increasing importance. In addition to low absorption at these wavelengths in clean air, the absorption due to water droplets, oil droplets and dust have recently been studied in wind tunnels.<sup>15</sup> The absorption was found to be an order of magnitude or more lower than for the commonly used wavelengths of 850, 1300 and 1550 nm. The present predicted speed is much higher than for directly modulated quantum cascade lasers. Continuous wave operation of a quantum cascade laser at room temperature has been demonstrated at  $\lambda = 9.2$   $\mu\text{m}$ .<sup>[16]</sup> When it comes to interband modulators at mid-IR wavelengths it appears that the research activities have been quite low so far.

The concept is also very promising for fiber-optical communication wavelengths like  $\lambda = 1.55$   $\mu\text{m}$ . This implementation requires material pairs with very large conduction band offsets. Such materials are generally less mature resulting in clearly larger line widths  $\Gamma$ , but with continued improvement of sample quality they should become superior to present interband modulators.<sup>17</sup>

In conclusion we have measured efficient electroabsorption in InP-based step quantum well structures. Clear Stark shifts were observed with a bias of the order 1 V. The results indicate that a 30  $\mu\text{m}$  long modulator with a surface plasmon waveguide can reach a speed exceeding  $f_{3\text{dB}} \sim 100$  GHz.

The authors are grateful to A. Patel for growing the samples by MOVPE. We thank Stéphane Junique, Lars Sjökvist and Jens Zander for valuable discussions.

- 
- <sup>1</sup> H. C. Liu, in *Intersubband transitions in quantum wells: Physics and device applications I*, edited by H. C. Liu and F. Capasso (Academic Press, San Diego, 2000), p. 129.
  - <sup>2</sup> J. Faist, D. Hofstetter, M. Beck, T. Aellen, M. Rochat, and S. Blaser, *Proc. SPIE* **4651**, 274 (2002).
  - <sup>3</sup> R. J. Warburton, K. Weilhammer, C. Jabs, J. P. Kotthaus, M. Thomas, and H. Kroemer, *Physica E* **7**, 191 (2000).
  - <sup>4</sup> P. Holmström, *IEEE J. Quantum Electron.* **37**, 1273 (2001).
  - <sup>5</sup> R. P. G. Karunasiri, Y. J. Mii, and K. L. Wang, *IEEE Electron. Device Lett.* **11**, 227 (1990).
  - <sup>6</sup> H. C. Liu, C. Y. Song, A. SpringThorpe, and G. C. Aers, *Electron. Lett.* **39**, 1149 (2003).
  - <sup>7</sup> C. Sirtori, F. Capasso, J. Faist, and S. Scandolo, *Phys. Rev. B* **50**, 8663 (1994).
  - <sup>8</sup> L. Hedin and B. I. Lundqvist, *J. Phys. C: Solid State Phys.* **4**, 2064 (1971).

- <sup>9</sup> W. L. Bloss, *J. Appl. Phys.* **66**, 3639 (1989).
- <sup>10</sup> T. Ando, *Solid State Commun.* **21**, 133 (1977).
- <sup>11</sup> I. Vurgaftman, J. R. Meyer, and L. R. Ram-Mohan, *J. Appl. Phys.* **89**, 5815 (2001).
- <sup>12</sup> P. Jänes, P. Holmström, and U. Ekenberg, *IEEE J. Quantum Electron.* **38**, 178 (2002).
- <sup>13</sup> B. Jalali, *IEEE J. Lightwave Tech.* **24**, 4600 (2006).
- <sup>14</sup> For a review, see D. Killinger, *Optics & Photonics News*, Oct. 2002, p. 49.
- <sup>15</sup> R. Martini, C. Glazowski, E. A. Whittaker, W. W. Harper, Y.-F. Su, J. F. Shultz, C. Gmachl, F. Capasso, D. L. Sivco, and A. Y. Cho, *Proc. SPIE* **5359**, 196 (2004).
- <sup>16</sup> M. Beck, D. Hofstetter, T. Aellen, J. Faist, U. Oesterle, M. Illegems, E. Gini, and H. Melchior, *Science* **295**, 301 (2002).
- <sup>17</sup> P. Holmström, *IEEE J. Quantum Electron.* **42**, 810 (2006).